Research Article Vol. 10, No. 4 / 1 April 2020 / Optical Materials Express 1007
Optical Materials EXPRESS

Exciton photoluminescence of $CsPbBr_3$@SiO_2 quantum dots and its application as a phosphor material in light-emitting devices

CANRAN ZHANG,[1] HONGXIANG ZHANG,[1] RU WANG,[2] DAOTONG YOU,[2] WEI WANG,[1,3] CHUNXIANG XU,[2] AND JUN DAI[1,*]

[1]Department of Physics, Jiangsu University of Science and Technology, Zhenjiang 212003, China
[2]State Key Laboratory of Bioelectronics, Southeast University, Nanjing 210096, China
[3]School of Engineering and Physical Science, Heriot-Watt University, Edinburgh EH144AS, United Kingdom
*daijun@just.edu.cn

Abstract: In this report, we mainly investigate the optical property differences between $CsPbBr_3$@SiO_2 quantum dots (QDs) and $CsPbBr_3$ QDs. The photoluminescence demonstrates that $CsPbBr_3$@SiO_2 QDs and $CsPbBr_3$ QDs have similar exciton binding energy. Both $CsPbBr_3$ and $CsPbBr_3$@SiO_2 QDs present optical bandgaps and photoluminescence (PL) linewidth broadening as the temperature increases from 10 K to room temperature, which is attributed to the thermal expansion and electron-phonon coupling. The fitting results show that $CsPbBr_3$ and $CsPbBr_3$@SiO_2 QDs have the similar bandgap thermal expansion coefficient, but the $CsPbBr_3$@SiO_2 QDs have weaker electron-phonon interaction. Temperature-dependent time-resolved photoluminescence (TRPL) demonstrates that the PL lifetime increases with the temperature and $CsPbBr_3$@SiO_2 QDs have longer PL lifetime than $CsPbBr_3$ QDs after 110 K. In addition, the $CsPbBr_3$@SiO_2 QDs integrated on the blue light-emitting diode chip as green phosphor material show better thermal stability in ambient air.

1. Introduction

Recently, perovskites semiconductor materials have been widely explored for practical application in the field of optoelec-tronics, such as solar cells, [1–5] light-emitting diodes (LEDs), [6–8] photo-detectors [9–11] and lasing devices [12–17]. Compared with the intrinsic thermal instability of organic and organic-inorganic hybrid perovskites, all-inorganic perovskites $CsPbX_3$ (X = Cl, Br, and I) have higher chemical stability and exhibit a high photoluminescence quantum yield [18–21]. However, high-quantum yield Cl-based perovskite devices are difficult to obtain owing to the relatively high density of Cl vacancy defects, [22] and I-based perovskite material still cannot overcome its instability for its undesirable phase transition at room temperature and humidity sensitivity [23,24]. Among the $CsPbX_3$ perovskites family, green $CsPbBr_3$ shows much better quantum yield and thermal stability than $CsPbCl_3$ and $CsPbI_3$ [25–27]. Therefore, green light $CsPbBr_3$ optical devices attract tremendous attention. In recent years, $CsPbBr_3$ perovskite microstructures with different structures and morphologies have been prepared by different growth methods, such as $CsPbBr_3$ microwire, [14,28] microsphere, [12] microplate [13] and quantum dots [8,29]. The underlying optical physics on $CsPbBr_3$ perovskites are widely investigated to further understand this excellent semiconductor material. Zhang *et al.* firstly reported $CsPbBr_3$ perovskite microwire/plates grown by the vapor deposition method, the temperature-dependence of photoluminescence reveals the exciton-phonon interaction in the $CsPbBr_3$ microstructure [12,28]. Different from the $CsPbBr_3$ microstructures by vapor deposition method, $CsPbBr_3$ QDs can be easily prepared by chemical solution method and have been widely used in the field of light-emitting devices, [6,8,30,31] enhanced amplified spontaneous emission,

#389847 https://doi.org/10.1364/OME.389847
Journal © 2020 Received 5 Feb 2020; revised 9 Mar 2020; accepted 13 Mar 2020; published 18 Mar 2020

Optical Materials EXPRESS

[32,33] photocatalysis, [34] and so on. Since the first report on $CsPbBr_3$ QDs, [29] different methods like surface passivation and element doping have been proposed to realize the $CsPbBr_3$ QDs with high stability and high quantum yield [35–38]. Sun *et al.* built silica shells on the $CsPbBr_3$ QDs surface to form the $CsPbBr_3@SiO_2$ QDs, its air stability was greatly improved [8]. Until now, much work have been done to improve the $CsPbBr_3@SiO_2$ QDs and its LED device performance [36,39,40]. However, the photoluminescence property difference of the $CsPbBr_3$ and $CsPbBr_3@SiO_2$ QDs have not been compared. On the other hand, the PL decay process also determines the light-emitting device performance, most of the reported $CsPbBr_3$ PL decay properties were only investigated at room temperature by single photon counting method, [6,41,42] the decay profile of the whole PL band of $CsPbBr_3$ is rarely studied. It is also unclear whether the SiO_2 can affect the PL decay process of $CsPbBr_3$ QDs. Therefore, it is of significance to compare the effect of SiO_2 coating on the optical properties of the $CsPbBr_3$ QDs.

In this paper, we investigated the effects of SiO_2 coating on the optical properties of the $CsPbBr_3$ QDs. The temperature-dependent photoluminescence was measured from 10 K to room temperature, the PL band presents obvious blue shift and continuous widening as the temperature increases, the effect of SiO_2 coating on the phonon-related optical properties of $CsPbBr_3$ QDs were discussed. The temperature-dependent time-resolved PL was also measured by the streak camera, the effect of SiO_2 coating on the PL lifetime was revealed. Finally, $CsPbBr_3@SiO_2$ QDs shows better thermal stability in air ambient than $CsPbBr_3$ QDs when they are served as phosphor material on the light-emitting diode chips.

2. Experimental

2.1. Preparation of $CsPbBr_3$ and $CsPbBr_3@SiO_2$ perovskite quantum dots

Firstly, we prepare the pure $CsPbBr_3$ quantum dots. Cs_2CO_3 (1.25 mmol, 99.9%), oleic acid (OA) (1.25 mL, 99%) and 1-octadecene (ODE) (15 mL, 90%) were mixed into 100 mL three-neck flask and the mixture was dried for 1h at 120 °C under the protection of N_2. Then, the reaction temperature was increased to 160 °C with magnetic stirring until the reaction mixture became a transparent solution. After about 30 min reaction, the Cs_2CO_3 powder can be completely dissolved. The cesium oleate precursor is prepared. In a 100 mL three-neck flask, 0.2 mmol $PbBr_2$ was added, followed by the addition of 5 mL of ODE, the mixture was heated at 120 °C for 1h under the protection of N_2. Then, the reaction temperature was increased to 160 °C, OA (0.5 mL) and OAm (0.5 mL) were injected into the reaction. When the solution became clear, the Cs-oleate precursor (0.6 mL) was quickly injected. After 5 s, the reaction mixture was cooled down to room temperature by an ice−water bath for the next purification process. Finally, the obtained quantum dots raw product was centrifuged at 9000 rpm for 15 min. After centrifugation, the supernatant was poured out, and the $CsPbBr_3$ quantum dots deposited at the bottom of the centrifuge tube were redispersed in toluene. Then, the $CsPbBr_3$ quantum dots dispersion solution was centrifuged at 12000 rpm for 10 min. After the purification, the $CsPbBr_3$ quantum dots were stored as dispersion in hexane.

The similar method reported by Sun *et al*. was employed to prepare the $CsPbBr_3@SiO_2$ perovskite quantum dots [7]. Different from the production process of pure $CsPbBr_3$ quantum dots, after the $PbBr_2$ mixture was heated at 120 °C for 1 h under the protection of N_2, OA (0.5 mL), OAm (0.5 mL) together with APTES (1 mL) were slowly added. Also, when the solution became clear, the Cs-oleate precursor (0.6 mL) was quickly injected. Then, the flask was opened to the air with continuous stirring for 1.5 h at 50% humidity, then the $CsPbBr_3@SiO_2$ QDs solution can be obtained.

Optical Materials EXPRESS

2.2. Experimental methods of temperature-dependent PL and TRPL

The prepared $CsPbBr_3$ and $CsPbBr_3@SiO_2$ quantum dots solutions were spin-coated onto 1 cm×1 cm quartz glass substrate to obtain for temperature-dependent optical test. The temperature-dependent PL was measured by low temperature system (Janis 150c) and the spectrometer (SP 2500i, Acton) equipped with CCD. The samples were placed in a quartz container where the temperature was cooled down to 10 K by liquid Helium system, and the PL was collected as the temperature was changed from 10 K to room temperature, meanwhile, the temperature-dependent TRPL was measured by the streak camera (Optronis GmbH SC-10). In the PL experiment, the samples were excited by 325 nm femtosecond laser (pulse duration of 150 fs, repetition rate of 1 kHz). In order to observe the carrier dynamics behavior of the pure $CsPbBr_3$ QDs in more detail, we used a larger grating when measuring its TRPL spectra.

3. Results and discussion

Transmission electron microscope (TEM) observations on the $CsPbBr_3$ and $CsPbBr_3@SiO_2$ QDs are shown in Fig. 1(a-b), respectively. The morphology of the $CsPbBr_3$ and $CsPbBr_3@SiO_2$ QDs do not have any obvious differences, and the white arrows in Fig. 1(b) indicate the SiO_2 layer. As shown in the TEM image of the $CsPbBr_3$ and $CsPbBr_3@SiO_2$ QDs, the pure $CsPbBr_3$ QDs aggregate together with an average size of ~ 9 nm (Fig. 1(c)), however, the $CsPbBr_3@SiO_2$ QDs randomly scattered with better dispersion and larger particle size of ~ 20 nm (Fig. 1(d)). After coating the SiO_2, the size of the QDs has almost doubled. In addition, the High-resolution TEM (HRTEM) image in the inset of Fig. 1(a-b) further demonstrates that the $CsPbBr_3@SiO_2$ QDs show a similar crystal structure with the pure $CsPbBr_3$ QDs, indicating that the coating of the SiO_2 has no influence on the basic structure of the QDs. The pure $CsPbBr_3$ QDs and $CsPbBr_3@SiO_2$ QDs both show a lattice spacing of ~ 4.1 Å, which corresponds to the <100> face of the cubic $CsPbBr_3$ perovskite phase.

Figure 1(e) shows the X-ray diffraction (XRD) pattern of the $CsPbBr_3$ (blue line) and $CsPbBr_3@SiO_2$ QDs (green line). The $CsPbBr_3@SiO_2$ QDs show the similar additional diffraction peaks to the pure $CsPbBr_3$ QDs (PDF#54-0752). In addition, the FWHM of the XRD peaks of the $CsPbBr_3@SiO_2$ QDs are about a half of the pure $CsPbBr_3$ QDs which shows that the particle size of $CsPbBr_3@SiO_2$ QDs are twice as large as $CsPbBr_3$ QDs according to the Scherrer equation.

Figure 2(a-b) show the contour mapping of the temperature-dependent PL for $CsPbBr_3$ and $CsPbBr_3@SiO_2$ QDs from 10 K to 300 K, and their corresponding normalized temperature-dependent PL spectrum are shown in Fig. 2(f-g).

Two typical features can be easily identified: (1) The PL intensity decreases continuously and (2) PL peaks shifts to the shorter wavelength as the sample temperature increases from 10 K to 300 K. Figure 2(c) shows the relationship between the integrated PL intensity and the temperature (1000/T). The integrated PL intensity can be well fitted by the Arrhenius equation for semiconductor luminescent materials [43,44]:

$$I(T) = \frac{I_0}{1 + Ae^{-\frac{E_B}{K_B T}}} \tag{1}$$

Where I(T) and I(0) are the integrated PL intensities at the temperature T K and 0 K, respectively. A is a fitted constant, K_B is Boltzmann constant, and E_B is exciton binding energy. Here the exciton binding energy E_B of $CsPbBr_3$ QDs and $CsPbBr_3@SiO_2$ QDs can be fitted as 18.16 meV and 19.08 meV, respectively. This indicates that the SiO_2 coating can hardly affect the exciton binding energy.

As shown in Fig. 2(a, b), the PL center wavelength (λ_{center}) of the $CsPbBr_3$ QDs and $CsPbBr_3@SiO_2$ QDs present blue shift from 527 to 513 nm and from 537 to 523 nm, when

Optical Materials EXPRESS

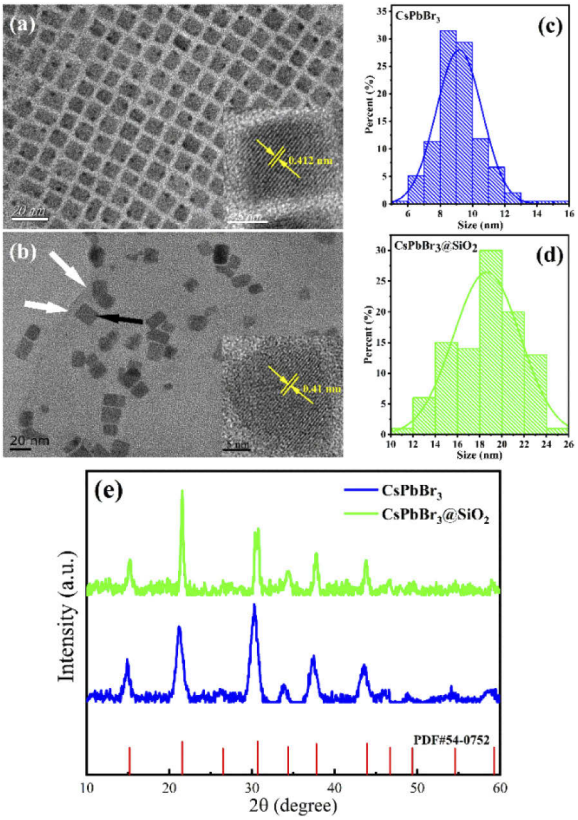

Fig. 1. (a) TEM of the $CsPbBr_3$ QDs. Scale bar is 20 nm. (inset: HRTEM of the $CsPbBr_3$ QDs. Scale bar is 5 nm.). (b) TEM of the $CsPbBr_3$@SiO_2 QDs. Scale bar is 20 nm. (inset: HRTEM of the $CsPbBr_3$@SiO_2 QDs. Scale bar is 5 nm.) The white arrows indicate SiO_2 layer, and the black arrow shows the QDs in SiO_2 matrix. (c-d) Size distribution of $CsPbBr_3$ and $CsPbBr_3$@SiO_2 QDs. (e) Standard XRD pattern of cubic phase PDF#54-0752.

the temperature increases from 10 K to 300 K. The $CsPbBr_3$ and $CsPbBr_3$@SiO_2 QDs present the same broadening of optical band gap E_g (Fig. 2(d)) from 10 K to 300 K, which is common for the inorganic $CsPbX_3$ (X= Br and I) perovskite as the temperature increases [41,42]. The temperature-dependent band gap can be written as [45]:

$$E_g(T) = E_0 + A_{TE}T + A_{EP}[\frac{2}{\exp(\hbar\omega/K_BT)-1} + 1] \quad (2)$$

where E_0 is the band gap at 0 K, A_{TE} is the thermal effect coefficient for band gap, A_{EP} is the electron-phonon coupling coefficient, $\hbar\omega$ is the average optical phonon energy. Four parameters can be fitted as $E_0 = 2.34$ eV, $A_{TE} = 0.389$ meV/K, $A_{EP} = -421$ meV, $\hbar\omega = 75$ meV for $CsPbBr_3$ QDs, and $E_0 = 2.30$ eV, $A_{TE} = 0.374$ meV/K, $A_{EP} = -167$ meV, $\hbar\omega = 52$ meV for $CsPbBr_3$@SiO_2 QDs. The $CsPbBr_3$ QDs always has wide band gap than that of $CsPbBr_3$@SiO_2 QDs, because the size of the $CsPbBr_3$ QDs are almost half of $CsPbBr_3$@SiO_2 QDs (see Fig. 1), the quantum size effect makes the smaller QDs have larger bandgap. In Fig. 2(d), the bandgap approximately linearly changes for $CsPbBr_3$ QDs when T is lower than 150 K, and for $CsPbBr_3$@SiO_2 QDs when T is lower than 120 K. The slopes of the linear band gap are similar for $CsPbBr_3$ and $CsPbBr_3$@SiO_2 QDs, which indicates that they have the similar thermal expansion coefficient A_{TE}. When the temperature is above 150 K, the bandgap of $CsPbBr_3$ QDs and $CsPbBr_3$@SiO_2 QDs increase with a decreasing slope and approaches to the maximum as the temperature increases

Optical Materials EXPRESS

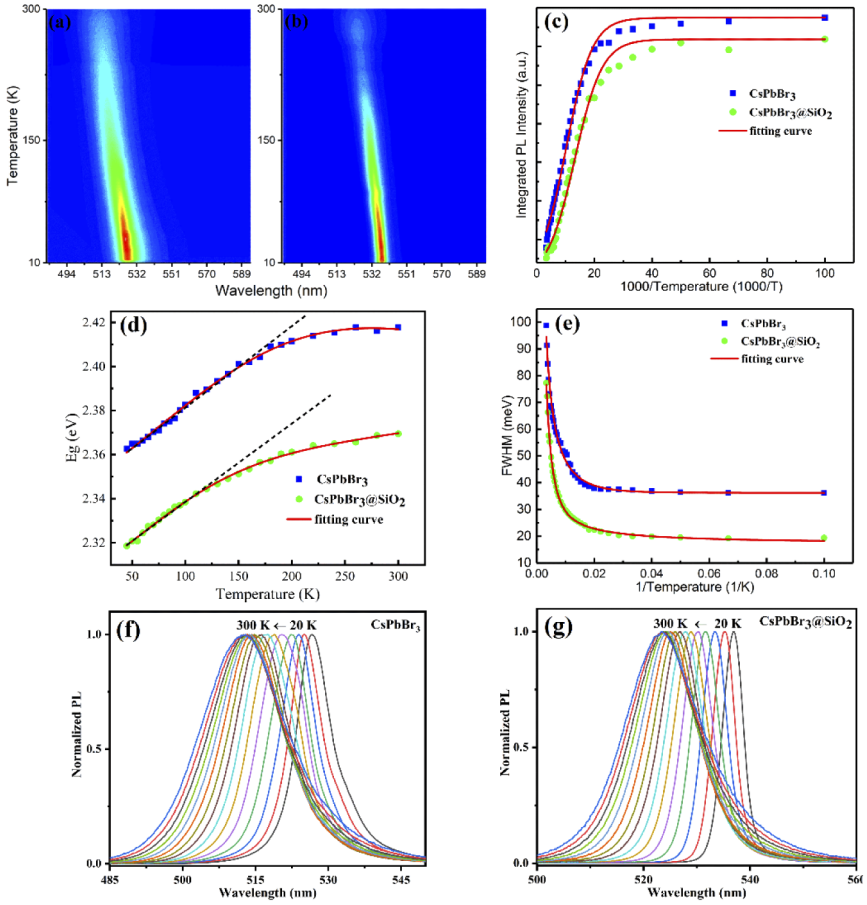

Fig. 2. Temperature-dependent PL mapping of (a) $CsPbBr_3$ QDs and (b) $CsPbBr_3@SiO_2$ QDs for the temperature region [10-300 K]. (c) The relationship of integrated PL intensity and 1000/temperature of $CsPbBr_3$ QDs and $CsPbBr_3@SiO_2$ QDs, respectively. The temperature-dependent (d) band gap and (e) PL FWHM of $CsPbBr_3$ QDs and $CsPbBr_3@SiO_2$ QDs, respectively. Normalized Temperature-dependent PL of (f) $CsPbBr_3$ QDs and (g) $CsPbBr_3@SiO_2$ QDs for the temperature region [20-300 K].

to room temperature. The sublinear behavior of the bandgap at high temperature (T > 150 K) originates from the synergistic effect of thermal expansion and electron-phonon interaction [28]. The result indicates that the electron-phonon interaction leading to the reduction of the band gap at high temperature. The lower electron-phonon coupling coefficient of $CsPbBr_3@SiO_2$ QDs indicates that the SiO_2 coating on the $CsPbBr_3$ QDs can decrease the electron-phonon coupling. The dielectric constant of matrix has strong effect on the strength of electron-phonon interaction [46]. We speculate that SiO_2 is an insulator that protects the QDs, the effect of the substrate and solution on QDs could be blocked, which leads to the decrease in electron-phonon coupling of $CsPbBr_3@SiO_2$ QDs. In addition, the magnitude of $\hbar\omega$ determines the temperature point at which the electron-phonon interaction starts to play the dominant role. The lower $\hbar\omega$ of the $CsPbBr_3@SiO_2$ QDs makes electron-phonon coupling effect occure at lower temperature of 120 K.

It is well known that the PL FWHM can be widened as the temperature increase. Here, the wider PL FWHM of $CsPbBr_3$ QDs without SiO_2 coating is due to the inhomogeneous quantum

Optical Materials EXPRESS

dots and homogeneous broadening originated from the stronger carrier-phonon interaction. It is considered that two kinds of phonon (acoustic phonon, longitudinal optical phonon) affect the PL band width [28,45]. Figure 2(e) shows the temperature-dependent FWHM on 1/Temperature of $CsPbBr_3$ and $CsPbBr_3$@SiO_2 QDs sample. The relationship between the FWHM and the temperature can be fitted by the following equation [28,45,47]:

$$\Gamma(T) = \Gamma_{inh} + \sigma T + \frac{\Gamma_{Lo}}{\exp(E_{LO}/k_B T)-1} \tag{3}$$

Where Γ_{inh} is the inhomogeneous band width caused by the inhomogenity of the sample, such as the size and shape of the quantum dots, σ is the exciton-acoustic phonon coupling coefficient. Γ_{LO} is the exciton-longitudinal (LO) mode optical phonon coupling coefficient. E_{LO} is the longitudinal mode optical phonon energy. The fitted parameters are Γ_{inh} = 31.75 meV, σ = 0.1703 meV/K, Γ_{LO} = 160.609 meV, E_{LO} = 65.05 meV for $CsPbBr_3$ QDs and Γ_{inh} = 17.1398 meV, σ = 0.11384 meV/K, Γ_{LO} = 100 meV, E_{LO} = 44.34 meV for $CsPbBr_3$@SiO_2 QDs. We can clearly see that the FWHM of the $CsPbBr_3$@SiO_2 QDs is about half smaller than $CsPbBr_3$ QDs and the Γ_{inh} of the $CsPbBr_3$@SiO_2 QDs is also half smaller than the $CsPbBr_3$ QDs as shown by Fig. 2(a-b) and Fig. 2(e), which indicates that the $CsPbBr_3$@SiO_2 QDs have better homogeneity in shape and surface roughness than the $CsPbBr_3$ QDs. In addition, the Γ_{LO} and E_{LO} of the $CsPbBr_3$@SiO_2 QDs are smaller than the $CsPbBr_3$ QDs, which consistent with the A_{EP} and $\hbar\omega$ in the bandgap fitting results. This result futher indicates that the SiO_2 coating on the $CsPbBr_3$ QDs can decrease the electron-phonon (especially LO phonon) coupling. The σ of $CsPbBr_3$ and $CsPbBr_3$@SiO_2 QDs are very small, suggesting that the exciton-acoustic phonon coupling contribution to the broadening of PL is weak [28,45]. The LO phonon energies are close to the average optical phonon energy $\hbar\omega$ fitted by Eq (2), suggesting that the LO phonon dominates the exciton-phonon interaction process [28].

In order to understand the carrier recombination dynamics at different temperature, the temperature dependent countering mapping TRPL of the $CsPbBr_3$ and $CsPbBr_3$@SiO_2 QDs were measured from 10 K to 200 K as shown in Fig. 3, and the vertical dimension of time range is 1400 ps for each slice. Figure 3(a-b) clearly shows that the carrier decay process is prolonged as the temperature increases from 10 to 200 K. The exact lifetime of the PL center increase from 160 ps to 340 ps for the $CsPbBr_3$ QDs, and from 50 ps to 410 ps for the $CsPbBr_3$@SiO_2 QDs, as shown in Fig. 4(a-b). For some inorganic semiconductor and $CsPbBr_3$ microstructures, the prolonged PL lifetime at higher temperature is also observed, which is attributed to the exciton thermal dissociation [48]. When the temperature is higher than 110 K, the PL lifetime of

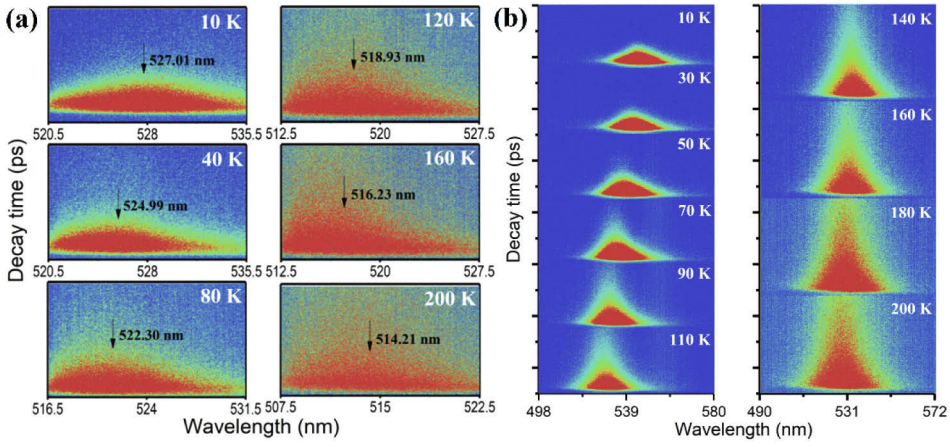

Fig. 3. TRPL of (a) $CsPbBr_3$ QDs and (b) $CsPbBr_3$@SiO_2 QDs at different temperature.

Optical Materials EXPRESS

$CsPbBr_3$@SiO_2 QDs is longer than that of $CsPbBr_3$ QDs, this indicates that $CsPbBr_3$@SiO_2 QDs are more suitable for light-emitting materials. In addition, the blueshift of the PL center (black arrow in Fig. 3(a)) can also be demonstrated on the TRPL spectra. Figure 4(c-d) show the representative TRPL of the PL center wavelength at 10, 50, 100, 150 and 200 K for $CsPbBr_3$ and $CsPbBr_3$@SiO_2 QDs, all of the TRPL present monoexponential decay process which corresponds to mono-exciton recombination process. Different from the reported $CsPbBr_3$ nanostructure with two exciton PL lifetime components (exciton, trapped exciton) [49] and Auger recombination, [50] the single PL lifetime of our sample indicates the high quality of the crystalline with few luminescent trap states [14,49].

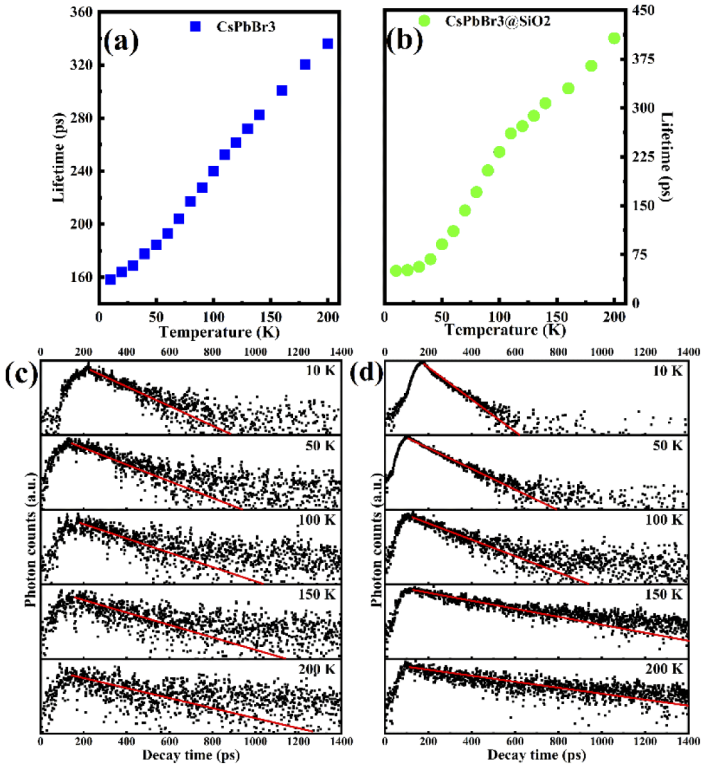

Fig. 4. The lifetime of the (a) $CsPbBr_3$ and (b) $CsPbBr_3$@SiO_2 QDs at different temperature.The decay process for the center PL wavelength at different temperatures of (c) $CsPbBr_3$ QDs and (d) $CsPbBr_3$@SiO_2 QDs.

To investigate the improvement of stability of the $CsPbBr_3$@SiO_2 QDs, we measured PL of the $CsPbBr_3$ QDs and $CsPbBr_3$@SiO_2 QDs in air ambient (Fig. 5(a-b)). When these samples were excited by 325 nm laser, the PL intensity of $CsPbBr_3$ QDs decreased to 40% of its original intensity after 16 days, while the PL intensity $CsPbBr_3$@SiO_2 QDs decreased much less than $CsPbBr_3$ QDs. Further $CsPbBr_3$ and $CsPbBr_3$@SiO_2 QDs were dried, we mixed them with silicone resin solution, respectively. Then the same mount $CsPbBr_3$/silicone resin and $CsPbBr_3$@SiO_2 QDs/silicone resin were dipped on LED chips and solidified after 1hour heating at 50 °C. As the LED is working and dissipating heat (surface temperature ≈ 70 °C), we then tested the thermal stability of $CsPbBr_3$ QDs and $CsPbBr_3$@SiO_2 QDs. Figure 5(c) and (d) show the PL spectra of the $CsPbBr_3$ and $CsPbBr_3$@SiO_2 QDs excited by the blue LED chip (λ_{center} = 450 nm). As can be seen from the inset of Fig. 5(c) and (d), at the same working current, the $CsPbBr_3$@SiO_2 QDs on the LED surface emit brighter light than the $CsPbBr_3$ QDs. After 12

Optical Materials EXPRESS

hours of continuous working, the PL intensity of the $CsPbBr_3@SiO_2$ QDs on the LED chip is hardly reduced. However, the PL intensity of $CsPbBr_3$ QDs on LED chip is reduced by 40% only after 60 minutes. This indicates that the $CsPbBr_3@SiO_2$ QDs show much better thermal stability when it is integrated on the LED chips.

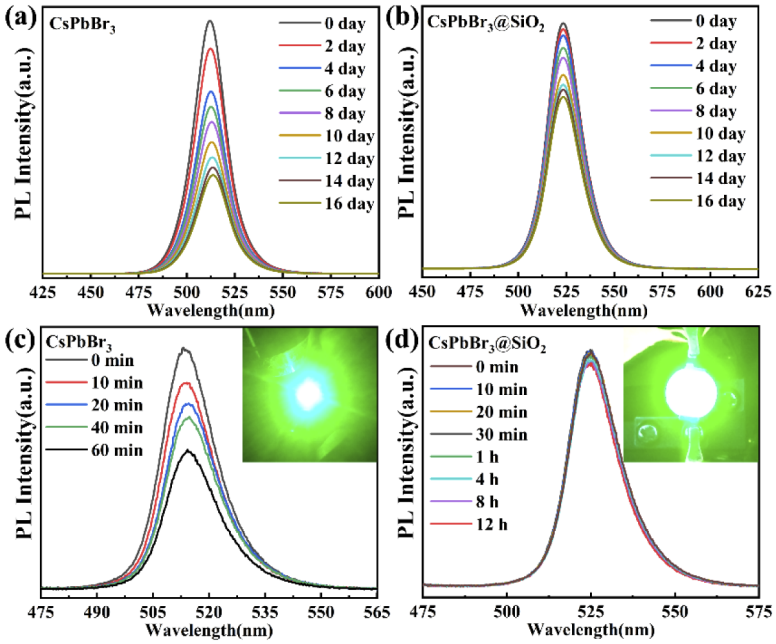

Fig. 5. (a-b) PL spectra of the $CsPbBr_3$ and $CsPbBr_3@SiO_2$ QDs measured at different working time. (c-d) PL spectra of the $CsPbBr_3$ and $CsPbBr_3@SiO_2$ QDs measured at different working time on blue LED chips.

4. Conclusion

In summary, the temperature-dependent PL and TRPL of $CsPbBr_3$ and $CsPbBr_3@SiO_2$ QDs were investigated. $CsPbBr_3@SiO_2$ QDs show the similar exciton binding energy as $CsPbBr_3$ QDs after SiO_2 coating. Both $CsPbBr_3$ and $CsPbBr_3@SiO_2$ QDs present continuous broadening of optical bandgap from 10 K to 300 K, the exact thermal expansion induced bandgap broadening and electron-phonon interaction induced bandgap narrowing were discussed, the result indicates that the electron-phonon coupling can be decreased in the $CsPbBr_3@SiO_2$ QDs. The temperature-dependent TRPL demonstrates that the PL lifetime increases with the temperature, and $CsPbBr_3@SiO_2$ QDs have longer PL lifetime than $CsPbBr_3$ QDs at high temperature. In addition, $CsPbBr_3@SiO_2$ QDs show better thermal stability in air ambient than $CsPbBr_3$ QDs when they were integrated on blue light-emitting diode chips. The above conclusions indicate that $CsPbBr_3@SiO_2$ QDs are more suitable for light-emitting materials.

Funding

National Natural Science Foundation of China (11874185, 11981240363); Qinglan Project of Jiangsu Province of China.

Disclosures

The authors declare no conflicts of interest.

Optical Materials EXPRESS

References

1. P. Y. Wang, X. W. Zhang, Y. Q. Zhou, Q. Jiang, Q. F. Ye, Z. M. Chu, X. X. Li, X. L. Yang, Z. G. Yin, and J. B. You, "Solvent-controlled growth of inorganic perovskite films in dry environment for efficient and stable solar cells," Nat. Commun. **9**(1), 2225 (2018).
2. S. H. Wu, R. Chen, S. S. Zhang, B. H. Babu, Y. F. Yue, H. M. Zhu, Z. C. Yang, C. L. Chen, W. T. Chen, Y. Q. Huang, S. Y. Fang, T. L. Liu, L. Y. Han, and W. Chen, "A chemically inert bismuth interlayer enhances long-term stability of inverted perovskite solar cells," Nat. Commun. **10**(1), 1161 (2019).
3. L. G. Wang, H. P. Zhou, J. N. Hu, B. L. Huang, M. Z. Sun, B. W. Dong, G. H. J. Zheng, Y. Huang, Y. H. Chen, L. Li, Z. Q. Xu, N. X. Li, Z. Liu, Q. Chen, L. D. Sun, and C. H. Yan, "A Eu^{3+}-Eu^{2+} ion redox shuttle imparts operational durability to Pb-I perovskite solar cells," Science **363**(6424), 265–270 (2019).
4. E. H. Jung, N. J. Jeon, E. Y. Park, C. S. Moon, T. J. Shin, T. Y. Yang, J. H. Noh, and J. Seo, "Efficient, stable and scalable perovskite solar cells using poly(3-hexylthiophene)," Nature **567**(7749), 511–515 (2019).
5. H. X. Wang, S. L. Cao, B. Yang, H. Y. Li, M. Wang, X. F. Hu, K. Sun, and Z. G. Zang, "NH4Cl-Modified ZnO for High-Performance $CsPbIBr_2$ Perovskite Solar Cells via Low-Temperature Process," Sol. RRL **4**, 1900363 (2020).
6. X. M. Li, Y. Wu, S. L. Zhang, B. Cai, Y. Gu, J. Z. Song, and H. B. Zeng, "CsPbX3 Quantum Dots for Lighting and Displays: Room-Temperature Synthesis, Photoluminescence Superiorities, Underlying Origins and White Light-Emitting Diodes," Adv. Funct. Mater. **26**, 2435–2445 (2016).
7. W. W. Chen, T. C. Shi, J. Du, Z. G. Zang, Z. Q. Yao, M. Li, K. Sun, W. Hu, Y. X. Leng, and X. S. Tang, "Highly Stable Silica-Wrapped Mn-Doped $CsPbCl_3$ Quantum Dots for Bright White Light-Emitting Devices," ACS Appl. Mater. Interfaces **10**(50), 43978–43986 (2018).
8. C. Sun, Y. Zhang, C. Ruan, C. Y. Yin, X. Y. Wang, Y. D. Wang, and W. W. Yu, "Efficient and Stable White LEDs with Silica-Coated Inorganic Perovskite Quantum Dots," Adv. Mater. **28**(45), 10088–10094 (2016).
9. J. G. Feng, C. Gong, H. F. Gao, W. Wen, Y. J. Gong, X. Y. Jiang, B. Zhang, Y. C. Wu, Y. S. Wu, H. B. Fu, L. Jiang, and X. Zhang, "Single-crystalline layered metal-halide perovskite nanowires for ultrasensitive photodetectors," Nat. Electron. **1**(7), 404–410 (2018).
10. C. X. Bao, J. Yang, S. Bai, W. D. Xu, Z. B. Yan, Q. Y. Xu, J. M. Liu, W. J. Zhang, and F. Gao, "Photodetectors: High Performance and Stable All-Inorganic Metal Halide Perovskite-Based Photodetectors for Optical Communication Applications," Adv. Mater. **30**, 1870288 (2018).
11. H. Zhou, J. P. Zeng, Z. N. Song, C. R. Grice, C. Chen, Z. H. Song, D. W. Zhao, H. Wang, and Y. F. Yan, "Self-Powered All-Inorganic Perovskite Microcrystal Photodetectors with High Detectivity," J. Phys. Chem. Lett. **9**(8), 2043–2048 (2018).
12. W. N. Du, S. Zhang, Z. Y. Wu, Q. Y. Shang, Y. Mi, J. Chen, C. C. Qin, X. H. Qiu, Q. Zhang, and X. F. Liu, "Unveiling lasing mechanism in $CsPbBr_3$ microsphere cavities," Nanoscale **11**(7), 3145–3153 (2019).
13. Q. Zhang, R. Su, X. F. Liu, J. Xing, T. C. Sum, and Q. H. Xiong, "High-Quality Whispering-Gallery-Mode Lasing from Cesium Lead Halide Perovskite Nanoplatelets," Adv. Funct. Mater. **26**, 6238–6245 (2016).
14. C. R. Zhang, J. J. Duan, F. F. Qin, C. X. Xu, W. Wang, and J. Dai, "$CsPbBr_3$ interconnected microwire structure: temperature-related photoluminescence properties and its lasing action," J. Mater. Chem. C **7**(34), 10454–10459 (2019).
15. X. X. Wang, M. Shoaib, X. Wang, X. H. Zhang, M. He, Z. Y. Luo, W. H. Zheng, H. L. Li, T. F. Yang, X. L. Zhu, L. B. Ma, and A. L. Pan, "High-Quality In-Plane Aligned $CsPbX_3$ Perovskite Nanowire Lasers with Composition-Dependent Strong Exciton–Photon Coupling," ACS Nano **12**(6), 6170–6178 (2018).
16. Q. Zhang, S. T. Ha, X. F. Liu, T. C. Sum, and Q. H. Xiong, "Room-Temperature Near-Infrared High-Q Perovskite Whispering-Gallery Planar Nanolasers," Nano Lett. **14**(10), 5995–6001 (2014).
17. X. X. Wang, H. Z. Chen, H. Zhou, X. Wang, S. P. Yuan, Z. Q. Yang, X. L. Zhu, R. M. Ma, and A. L. Pan, "Room-temperature high-performance $CsPbBr_3$ perovskite tetrahedral microlasers," Nanoscale **11**(5), 2393–2400 (2019).
18. Y. Bekenstein, B. A. Koscher, S. W. Eaton, P. D. Yang, and A. P. Alivisatos, "Highly Luminescent Colloidal Nanoplates of Perovskite Cesium Lead Halide and Their Oriented Assemblies," J. Am. Chem. Soc. **137**(51), 16008–16011 (2015).
19. A. Swarnkar, R. Chulliyil, V. K. Ravi, M. Irfanullah, A. Chowdhury, and A. Nag, "Colloidal $CsPbBr_3$ Perovskite Nanocrystals: Luminescence beyond Traditional Quantum Dots," Angew. Chem. **127**(51), 15644–15648 (2015).
20. D. D. Zhang, S. W. Eaton, Y. Yu, L. T. Dou, and P. D. Yang, "Solution-Phase Synthesis of Cesium Lead Halide Perovskite Nanowires," J. Am. Chem. Soc. **137**(29), 9230–9233 (2015).
21. M. C. Brennan, J. E. Herr, T. S. Nguyen-Beck, J. Zinna, S. Draguta, S. Rouvimov, J. Parkhill, and M. Kuno, "Origin of the Size-Dependent Stokes Shift in $CsPbBr_3$ Perovskite Nanocrystals," J. Am. Chem. Soc. **139**(35), 12201–12208 (2017).
22. M. I. Saidaminov, M. A. Haque, M. Savoie, A. L. Abdelhady, N. Cho, I. Dursun, U. Buttner, E. Alarousu, T. Wu, and O. M. Bakr, "Perovskite Photodetectors Operating in Both Narrowband and Broadband Regimes," Adv. Mater. **28**, 8144–8149 (2016).
23. R. J. Sutton, G. E. Eperon, L. Miranda, E. S. Parrott, B. A. Kamino, J. B. Patel, M. T. Hörantner, M. B. Johnston, A. A. Haghighirad, D. T. Moore, and H. J. Snaith, "Bandgap-Tunable Cesium Lead Halide Perovskites with High Thermal Stability for Efficient Solar Cells," Adv. Energy Mater. **6**(8), 1502458 (2016).

Optical Materials EXPRESS

24. A. Swarnkar, A. R. Marshall, E. M. Sanehira, B. D. Chernomordik, D. T. Moore, J. A. Christians, T. Chakrabarti, and J. M. Luther, "Quantum dot–induced phase stabilization of α-$CsPbI_3$ perovskite for high-efficiency photovoltaics," Science **354**(6308), 92–95 (2016).
25. Y. P. Fu, H. M. Zhu, C. C. Stoumpos, Q. Ding, J. Wang, M. G. Kanatzidis, X. Y. Zhu, and S. Jin, "Broad Wavelength Tunable Robust Lasing from Single-Crystal Nanowires of Cesium Lead Halide Perovskites ($CsPbX_3$, X = Cl, Br, I)," ACS Nano **10**(8), 7963–7972 (2016).
26. K. Park, J. W. Lee, J. D. Kim, N. S. Han, D. M. Jang, S. Jeong, J. Park, and J. K. Song, "Light–Matter Interactions in Cesium Lead Halide Perovskite Nanowire Lasers," J. Phys. Chem. Lett. **7**(18), 3703–3710 (2016).
27. W. Du, S. Zhang, J. Shi, J. Chen, Z. Y. Wu, Y. Mi, Z. X. Liu, Y. Z. Li, X. Y. Sui, R. Wang, X. H. Qiu, T. Wu, Y. F. Xiao, Q. Zhang, and X. F. Liu, "Strong Exciton–Photon Coupling and Lasing Behavior in All-Inorganic $CsPbBr_3$ Micro/Nanowire Fabry-Pérot Cavity," ACS Photonics **5**(5), 2051–2059 (2018).
28. Z. Liu, Q. Y. Shang, C. Li, L. Y. Zhao, Y. Gao, Q. Li, J. Chen, S. Zhang, X. F. Liu, Y. S. Fu, and Q. Zhang, "Temperature-dependent photoluminescence and lasing properties of $CsPbBr_3$ nanowires," Appl. Phys. Lett. **114**(10), 101902 (2019).
29. L. Protesescu, S. Yakunin, M. I. Bodnarchuk, F. Krieg, R. Caputo, C. H. Hendon, R. X. Yang, A. Walsh, and M. V. Kovalenko, "Nanocrystals of Cesium Lead Halide Perovskites ($CsPbX_3$, X = Cl, Br, and I): Novel Optoelectronic Materials Showing Bright Emission with Wide Color Gamut," Nano Lett. **15**(6), 3692–3696 (2015).
30. C. L. Li, Z. G. Zang, W. W. Chen, Z. P. Hu, X. S. Tang, W. Hu, K. Sun, X. M. Liu, and W. M. Chen, "Highly pure green light emission of perovskite $CsPbBr_3$ quantum dots and their application for green light-emitting diodes," Opt. Express **24**(13), 15071–15078 (2016).
31. H. L. Guan, S. Y. Zhao, H. X. Wang, D. D. Yan, M. Wang, and Z. G. Zang, "Room temperature synthesis of stable single silica-coated $CsPbBr_3$ quantum dots combining tunable red emission of Ag–In–Zn–S for High-CRI white light-emitting diodes," Nano Energy **67**, 104279 (2020).
32. D. D. Yan, T. C. Shi, Z. G. Zang, T. W. Zhou, Z. Z. Liu, Z. Y. Zhang, J. Du, Y. X. Leng, and X. S. Tang, "Ultrastable $CsPbBr_3$ Perovskite Quantum Dot and Their Enhanced Amplified Spontaneous Emission by Surface Ligand Modification," Small **15**, 1901173 (2019).
33. Z. P. Hu, Z. Z. Liu, Y. Bian, S. Q. Li, X. S. Tang, J. Du, Z. G. Zang, M. Zhou, W. Hu, Y. X. Tian, and Y. X. Leng, "Enhanced Two-Photon-Pumped Emission from In Situ Synthesized Nonblinking $CsPbBr_3/SiO_2$ Nanocrystals with Excellent Stability," Adv. Opt. Mater. **6**, 1700997 (2018).
34. Y. F. Xu, M. Z. Yang, B. X. Chen, X. D. Wang, H. Y. Chen, D. B. Kuang, and C. Y. Su, "A $CsPbBr_3$ Perovskite Quantum Dot/Graphene Oxide Composite for Photocatalytic CO_2 Reduction," J. Am. Chem. Soc. **139**(16), 5660–5663 (2017).
35. J. H. Li, L. M. Xu, T. Wang, J. Z. Song, J. W. Chen, J. Xue, Y. H. Dong, B. Cai, Q. S. Shan, B. N. Han, and H. B. Zeng, "50-Fold EQE Improvement up to 6.27% of Solution-Processed All-Inorganic Perovskite $CsPbBr_3$ QLEDs via Surface Ligand Density Control," Adv. Mater. **29**(5), 1603885 (2017).
36. D. Q. Chen, G. L. Fang, and X. Chen, "Silica-Coated Mn-Doped $CsPb(Cl/Br)_3$ Inorganic Perovskite Quantum Dots: Exciton-to-Mn Energy Transfer and Blue-Excitable Solid-State Lighting," ACS Appl. Mater. Interfaces **9**(46), 40477–40487 (2017).
37. S. Li, Z. F. Shi, F. Zhang, L. T. Wang, Z. Z. Ma, D. W. Yang, Z. Q. Yao, D. Wu, T. T. Xu, Y. T. Tian, Y. T. Zhang, C. X. Shan, and X. J. Li, "Sodium Doping-Enhanced Emission Efficiency and Stability of $CsPbBr_3$ Nanocrystals for White Light-Emitting Devices," Chem. Mater. **31**(11), 3917–3928 (2019).
38. D. D. Yang, X. M. Li, W. H. Zhou, S. L. Zhang, C. F. Meng, Y. Wu, Y. Wang, and H. B. Zeng, "$CsPbBr_3$ Quantum Dots 2.0: Benzenesulfonic Acid Equivalent Ligand Awakens Complete Purification," Adv. Mater. **31**, 1900767 (2019).
39. Q. X. Zhong, M. H. Cao, H. C. Hu, D. Yang, M. Chen, P. L. Li, L. Z. Wu, and Q. Zhang, "One-Pot Synthesis of Highly Stable $CsPbBr_3$@SiO2 Core–Shell Nanoparticles," ACS Nano **12**(8), 8579–8587 (2018).
40. X. M. Li, Y. Wang, H. D. Sun, and H. B. Zeng, "Amino-Mediated Anchoring Perovskite Quantum Dots for Stable and Low-Threshold Random Lasing," Adv. Mater. **29**(36), 1701185 (2017).
41. R. Saran, A. Heuer-Jungemann, A. G. Kanaras, and R. J. Curry, "Giant Bandgap Renormalization and Exciton–Phonon Scattering in Perovskite Nanocrystals," Adv. Opt. Mater. **5**(17), 1700231 (2017).
42. A. Shinde, R. Gahlaut, and S. Mahamuni, "Low-Temperature Photoluminescence Studies of $CsPbBr_3$ Quantum Dots," J. Phys. Chem. C **121**(27), 14872–14878 (2017).
43. H. G. Zheng, J. Dai, J. J. Duan, F. Chen, G. Y. Zhu, F. Wang, and C. X. Xu, "Temperature-dependent photoluminescence properties of mixed-cation methylammonium–formamidium lead iodide $[HC(NH_2)_2]_x[CH_3NH_3]_{1-x}PbI_3$ perovskite nanostructures," J. Mater. Chem. C **5**(46), 12057–12061 (2017).
44. D. S. Jiang, H. Jung, and K. Ploog, "Temperature dependence of photoluminescence from GaAs single and multiple quantum-well heterostructures grown by molecular-beam epitaxy," J. Appl. Phys. **64**(3), 1371–1377 (1988).
45. K. Wei, Z. J. Xu, R. Z. Chen, X. Zheng, X. G. Cheng, and T. Jiang, "Temperature-dependent excitonic photoluminescence excited by two-photon absorption in perovskite $CsPbBr_3$ quantum dots," Opt. Lett. **41**(16), 3821–3824 (2016).
46. B. Ai, C. Liu, Z. Deng, J. Wang, J. J. Han, and X. J. Zhao, "Low temperature photoluminescence properties of $CsPbBr_3$ quantum dots embedded in glasses," Phys. Chem. Chem. Phys. **19**(26), 17349–17355 (2017).

Optical Materials EXPRESS

47. J. Lee, E. S. Koteles, and M. O. Vassell, "Luminescence linewidths of excitons in GaAs quantum wells below 150 K," Phys. Rev. B **33**(8), 5512–5516 (1986).
48. M. C. Tam, A. M. C. Ng, A. B. Djurišić, and K. S. Wong, "Correlation of quantum efficiency and photoluminescence lifetime of ZnO tetrapods grown at different temperatures," J. Appl. Phys. **112**(2), 023515 (2012).
49. J. Dai, Y. Fu, L. H. Manger, M. T. Rea, L. Hwang, R. H. Goldsmith, and S. Jin, "Carrier Decay Properties of Mixed Cation Formamidinium–Methylammonium Lead Iodide Perovskite $[HC(NH_2)_2]_{1-x}[CH_3NH_3]_xPbI_3$ Nanorods," J. Phys. Chem. Lett. **7**(24), 5036–5043 (2016).
50. Q. Y. Li, Y. W. Yang, W. X. Que, and T. Q. Lian, "Size- and Morphology-Dependent Auger Recombination in $CsPbBr_3$ Perovskite Two-Dimensional Nanoplatelets and One-Dimensional Nanorods," Nano Lett. **19**(8), 5620–5627 (2019).